Supplementary Materials for

The Connectome of a Decision-Making Neural Network

Travis A. Jarrell, Yi Wang, Adam E. Bloniarz, Christopher A. Brittin, Meng Xu, J. Nichol Thomson, Donna G. Albertson, David H. Hall, Scott W. Emmons*

To whom correspondence should be addressed. E-mail: scott.emmons@einstein.yu.edu

Published 27 July 2012, *Science* **337**, 437 (2012)
DOI: 10.1126/science.1221762

This PDF file includes:

Other Supplementary Material for this manuscript includes the following:
(available at www.sciencemag.org/cgi/content/full/337/6093/437/DC1)

Movie S1

Other Supplementary Material for this manuscript includes the following:
(available from the author, http://worms.aecom.yu.edu/jarrelletalSOM.html and as linked below)

Database S1: Anatomical localization of the N2Y electron micrographic series.

Database S2: The electron micrographs of the N2Y series. The Worm Image Database and Open Connectome Project

Database S3: The raw data describing the annotations of the electron micrographs recorded with Elegance.

Database S4: Synapse lists for each neuron and muscle and neuron maps.

Database S5: List of neurons.

Database S6: List of muscles.

Database S7: List of neurons uninvolved in the mating circuits.

Database S8: Adjacency matrix of chemical connections in the N2Y database used for analyzing the networks for the present publication

Database S9: Adjacency matrix of gap junction connections in the N2Y database used for analyzing the networks for the present publication.

Materials and Methods

Electron microscopy. The electron micrographs (EMs) used in this study were originally prepared as part of the first reconstructions of nervous system connectivity in *C. elegans* by J. G. White, S. Brenner, and co-workers at the MRC in Cambridge, England, beginning in the 1970s. Details of sample preparation and electron microscopy are given in their publication (*1*). Briefly, nematodes grown on bacteria on agar plates were fixed in 1% osmium tetroxide, embedded in Araldite, sectioned, and stained with uranyl acetate and lead citrate after mounting on Formvar coated grids.

The N2Y series. The series of approximately 5,000 thin sections from which our reconstruction was made is called the N2Y series (*1*). Section thickness is 70-90 nm, judged from section color (silver) (*48*) and nematode anatomy. EMs were previously analyzed in a study of male ultrastructure, where the series is described as Series 4 (*10*). The N2Y animal sectioned is of the Bristol strain N2 and is described as an "old adult" (there is no further information as to how "old") (*10*). The Cambridge micrographs consist of 385 low-power images containing an entire worm cross section taken every 10 to 20 sections extending from midbody through to the tail tip, and several sets of high-power images taken every 1 to 3 sections covering regions containing neuron processes (Fig. S1; see also database S1). For the present study, the original 12-in × 16-in paper prints were digitized into 40 mb TIFF files for analysis on the computer screen.

Identification of neurites. EMs were annotated, and the connectome was assembled using the software platform Elegance (open source, available at https://github.com/Emmonslab). The identity of most neurites was obtained when they were traced to a cell body of known identity. Many cell bodies—for example, those in the pre-anal ganglion—are identifiable from their

reproducible positions (*10*). This is not the case for cell bodies in the lumbar ganglia, which assume variable positions during morphogenesis of the tail at the L4 to adult molt. Ray neuron cell bodies in the lumbar ganglia were identified by tracing their dendritic processes to the rays. The remaining lumbar cells, which are shared with the hermaphrodite, were identified in part by comparison with hermaphrodite connectivity. Unambiguous connection of neurites in the pre-anal ganglion through commissures to their cell bodies in other ganglia could not be made in all cases. In such instances, identification could usually be made by a process of elimination when bundles of processes entering and exiting a commissure were reconciled, or by comparing the connectivity of opposite-side homologs. An additional source of uncertainty in neurite identification in the N2Y series is due to an apparently missing grid, creating a gap of about 30 high-power images just before the ventral cord expands into the pre-anal ganglion. It was difficult in some cases to correlate processes extending across this gap from the most-posterior image in the ventral cord series to the most-anterior image in the pre-anal ganglion series. Finally, muscle arms were not always traced to the muscle of origin, which was simply taken to be the nearest muscle.

The cellular identities of neurites not traced to an unambiguously identified cell body or securely determined by some other means, yet nevertheless reasonably certain, are indicated in brackets in the synapse lists. Their contribution to connectivity is included in the adjacency matrices. In the end, the identities of 317 different neurite fragments could not be determined. These have a combined total length of 16,559 sections (6.5% of the total) and contribute to 6.6% of the total number of sections of chemical synapses and 5.2% of the total number of sections of gap junctions scored. They are identified as unk (unknown) on the synapse lists and make no contribution to the adjacency matrices.

Scoring synapses and synapse size. The appearance in *C. elegans* EMs of chemical synapses, neuromuscular junctions, and gap junctions has been described (*1*). In Elegance, the X, Y, Z (section number) coordinate of each pre-synaptic density and gap junction is recorded on each image. Objects that denote synaptic structures running through multiple sections are connected together. Thus both the number and locations of individual synapses and their sizes, in number of serial sections, are obtained. Estimation of synapse size by counting the number of traversed serial sections is generally sufficient in *C. elegans* because, as *C. elegans* is a worm, outside of the nerve ring most of its neuronal processes run parallel to the longitudinal axis and are cut transversely in the serial sections. Synapses are en passant so that most of the difference in synapse size is captured by the number of serial sections they cross. Some information about variation in size in the X, Y plane of the micrograph is recorded during annotation (small, medium, large) but was not utilized in calculating total synapse size.

Calculation of vertex similarity. In order to assess the similarity of the connectivity of two neurons, we developed and used a formula for comparing the connectivity of two vertices in a weighted, directed graph that gives a more intuitive result in our application than standard and published procedures, as follows. Given a weighted, directed graph $G = (V,E)$ with adjacency matrix $\mathbf{A}_{ij}$, we consider vertices i,j in V to be similar if they have similarly weighted output to the same targets and similarly weighted input from the same sources. The conventional way to account for the similarity of targets is to take the inner product of rows i and j of $\mathbf{A}_{ij.}$ Intuitively, this says, for each vertex k in V in the graph, multiply the weight of the edge from i to k with the weight from j to k, and then sum over all k. Similarly, we take the inner product of columns to account for similarity with respect to inputs to the nodes. This method underlies cosine similarity and Tanimoto similarity, as well as the algorithm of Blondel *et al.* (*49*).

Instead of using the product of edge weights, we design a function that has properties that correspond more intuitively to a 'similarity score' on our datasets. Take for example the case where

$$\mathbf{A}_{ik} = 1$$

$$\mathbf{A}_{jk} = 100$$

This would add $100 = 1 \times 100$ to the inner product, whereas, if $\mathbf{A}_{ik}$ were 0, it would add 0, even though weights of 0 and 1, which in our datasets indicate the presence of a synapse in no or only a single EM serial section, may be biologically equivalent, both indicating a low probability of synapse formation. If $\mathbf{A}_{ik}$ were *either* 0 or 1, we would like this case to decrease the similarity score, since the weights $\mathbf{A}_{ik}$ and $\mathbf{A}_{jk}$ are so different. Thus, we design a function of the two numbers that can take negative values and will not be so different for the kinds of cases outlined above, and such that, for all x:

$f(0,x) < 0$, and as x decreases, so does the absolute value of $f(0,x)$

$f(x,x) = x$ as x gets large

A function that fulfills these criteria is:

$$f(x,y) = \min(x,y) - C_1 \max(x,y) e^{[-C2\min(x,y)]}$$

where x and y are the values $\mathbf{A}_{ik}$, $\mathbf{A}_{jk}$ and the overall similarity score for vertices i and j is the sum of $f(x,y)$ over all k.

C_1 determines how negatively we want to punish a case such as the one above. We use $C_1 = 0.5$, so that $f(0,100) = -50$. C_2 determines the point where the similarity of the two numbers switches from negative to positive. We use $C_2 = 1$, so that 100 and 2 are negatively similar, whereas 100 and 3 are slightly positively similar.

Graph analysis. The graph properties clustering coefficient and characteristic path length were calculated by creating a Boolean graph from the adjacency matrix and, for the chemical matrix, symmetrizing the connections; that is, the graphs were treated as unweighted, undirected graphs. For statistical analysis, the actual graphs were randomized by edge swapping so that the degree sequence was conserved.

Community analysis. Network community structure was analyzed using the modularity maximization spectral algorithm of Leicht and Newman (*20*). Neurons considered to be uninvolved in mating (database S7); interneurons EF1, EF2, and EF3; and hypodermis (hyp) were excluded. Muscles in functional groups were combined and treated as single nodes.

Motif analysis. The frequencies of doublets and triplets and tests for statistical significance were carried out following the procedures in Reigl *et al*. (*50*).

Supplementary Text: Results

The *C. elegans* male posterior nervous system. The overall structure and organization of the adult male posterior nervous system has been described (*10*). While the neuronal cell bodies are distributed in several ganglia (Fig. 1D), most of the synaptic connectivity is in the pre-anal

ganglion, although there are also synapses, particularly of the ray neurons, in the lumbar ganglia. The male-specific complement of neurons is born during the L3 and early L4 larval stages (*10*) and sends out processes to make connections, both with the pre-existing, shared nervous system and with other male-specific neurons, during L4 (*10*, *51*). This necessity to find synaptic targets in an already complex and continuously evolving neural region—in many cases, located in a different ganglion widely separated from the cell body—gives the male posterior neuropil a feature unlike the hermaphrodite nervous system and more similar to nervous systems in more complex animals, namely, branched neurons. Whereas the hermaphrodite nervous system is characterized by having mostly monopolar neurons that run in highly conserved neighborhoods (*1*, *52*), male-specific neurites appear to traverse many neighborhoods and branch, at times unproductively, in many directions. The pre-anal ganglion presents a complex tangle of neurites and indeed its appearance in cross section is nearly indistinguishable in the electron microscope from a section at the same magnification of mammalian brain tissue.

The connectome, availability of data, accuracy of reconstruction and synaptic weights. EMs and their annotations, neuron maps and synapse lists are available as databases S2 to S4. Lists of all the neurons and muscles mapped in N2Y and shown on the adjacency matrices are given in databases S5 and S6. The neurons that are thought not to play a significant role in the control of mating behavior are listed in database S7. The adjacency matrices of chemical and gap-junction connections in N2Y are databases S8 and S9.

The adjacency matrices represent our best estimate for the complete connectome. All the connections shown were observed, with two exceptions involving muscles. First, muscle arms were not always traced to a muscle body, which was assigned to be the nearest cell. Second, some gap junctions between muscles were not observed because no high-power EMs covered the

relevant regions. In these cases, knowing the consistency of these connections from reconstructed regions, we added gap junctions to the adjacency matrix where they are expected to connect adjacent muscle cells.

Multiple independent reconstructions showed the errors in the weights in the adjacency matrices are approximately independent of weight value and fall from around 10% for weights of 10 sections or less to 2% for edge weights of 40 sections or more. Error arises chiefly from ambiguous structures in the EMs that cause uncertainty as to the presence or absence of a pre-synaptic density or gap junction and the identity of post-synaptic partners at polyads.

Number and sizes of synapses. As elsewhere in the *C. elegans* nervous system, synapses are formed en passant. Pre- and postsynaptic chemical connections are interspersed along neuron processes consistent with graded-potential neurons (Fig. 1G). There being generally no visible post-synaptic specialization in *C. elegans*, postsynaptic cells are identified by their proximity to the presumptive neurotransmitter release site, defined by the presynaptic density and synaptic vesicles in the presynaptic cell. Fifty-nine percent of the chemical synapses are polyadic, that is, there is more than one possible postsynaptic partner. The identities of secondary postsynaptic cells at polyads is sometimes uncertain.

Both presynaptic densities and gap junctions vary in size over a continuous range, covering from 1 up to 41 sections for chemical synapses and from 1 to 30 sections for gap junctions (Fig. S2). The appearance of both pre-synaptic densities and gap junctions is similar for all cell types. The number of individual synapses connecting pairs of cells ranged from 1 to 64 for chemical synapses and from 1 to 26 for gap junctions, also with smooth distributions (Fig. S2).

The graphs of chemical and gap junction synapses are small-world networks. Characteristic of small-world networks, the graphs of chemical connections and gap junction connections between the neurons have high clustering coefficients and low characteristic path lengths (though statistically higher than randomized graphs) (Table S1). Combining the two graphs increases the clustering coefficient and decreases the characteristic path length only modestly, consistent with the overlap of the two graphs (Fig. S3). The gap-junction network connecting the muscles has a higher clustering coefficient, but also a significantly higher characteristic path length, which reflects the chainlike arrangement of the muscle systems attached to the body wall.

Left/right homologs have similar connectivity. The distributions of connection similarity scores for the neurons in pairwise comparisons are given in Fig. S4. Scores for left/right homologous neurons are greater than the scores for most non-left/right homologs. This is true for both chemical and gap-junction connections and even when only connections of 10 sections or less are used to make the comparison. Thus, left/right homologs, which are presumptively equivalent cells, make strong connections to similar sets of cells and weak connections to similar, different sets of cells.

Non-left/right neurons with apparently equivalent connectivity. A number of neuron pairs had connectivity similarity scores as high as left/right homologs, which defined groups of cells with similar patterns of connectivity. In every case, these were neurons that also had similar lineage ancestry, similar neurotransmitter expression, or similar genetic specification consistent with their being equivalent cells. Such pairs or groups of cells were usually reciprocally connected by chemical and gap-junction synapses. There are 41 neurons falling into nine groups that are taken to be equivalent by these criteria (Fig. S5).

Community structure of the network. Fig. 5 of the paper gives the set of five communities derived by the method of Leicht and Newman for the weighted, directed graph of chemical connections (*20*). The set of four communities obtained by the same method for the sensory neurons alone plus the type Ib interneurons, considering their chemical connections plus their gap-junction connections weighted by 0.5, is given in Fig. S6. For the entire network, the method of simulated annealing gave two communities, one comprising the neurons and muscles of the Response and Ejaculation modules, the other the remaining Leicht-Newman modules, PVV, R(1-5)A, and Locomotion (Fig. S7) (*53*). The iterative method of Ruan and Zhang subdivided the Leicht-Newman network into 27 subcommunities averaging five neurons per community (*54*). The method of Ahn *et al*. for defining communities by edges rather than nodes generated 157 communities of links and 245 communities of nodes (nodes can be in more than one community by this method) (*55*). The eleven communities discovered by the random walk method of Rosvall and Bergstrom are shown in Fig. S8 (*56*). The method of functional cartography partitioned the network as shown in Fig. S9 (*53*).

The partitions obtained with the various methods differed in detail. Some of these differences were meaningful, as for example when a neuron was grouped with its pre-synaptic partners in one community by one method and with its post-synaptic partners in a different community by another method. For some neurons, their assignment to one community or another was strongly sensitive to the inclusion or exclusion of other neurons in the analysis. Such sensitive behavior is often seen for algorithms that attempt to obtain an optimal partitioning and results from the lack of a clear global maximum (*57*). The most meaningful partitioning of the chemical graph, shown in Fig. 5, was obtained when the large, male-specific interneurons EF1, EF2, and EF3 and the hypodermis were excluded from the analysis. The EF neurons are

exclusively post-synaptic in the tail and communicate to the head through the ventral nerve cord. All the ray B-type sensory neurons (R[1-9]B[L/R]) are so strongly targeted to the EF neurons that inclusion of the EF neurons disrupts the partitions that divide the ray sensory neurons into meaningful sensory fields. The effect of moving the ray B neurons to a community with the EF neurons then radiates through the other communities and affects additional neurons.

In contrast to the volatile behavior of some neurons, a subset of core neurons and muscle groups were robustly clustered together and firmly characterized the same basic set of five communities. These neurons and muscle groups were *Response* module—R2B(L/R), R4B(L/R), R8B(L/R), PVY, PVX, LUA(L/R); *Locomotion* module—AVA(L/R), gender-shared body wall motor neurons, ventral body wall muscles; *R(1-5)A* module—A-type neurons of anterior rays (ray 1-5), diagonal muscles, longitudinal muscles; *PVV* module—PVV, PDA, PDB, PDC, AS11, CP07, CP08, CP09, dorsal body wall muscles; and *Insemination* module—PCB(L/R), PCC(L/R), SPC(L/R), CP01, CP02, CP03, CP04, CP05, CP06, anal depressor and spicule protractors, and gonad.

Overrepresentation of feedforward loop motifs. The frequencies of three-node motifs in the graph of chemical connections are compared with expected frequencies for randomized graphs in Fig. S10. Values are remarkably similar to those of the hermaphrodite (*2*).

Model of network function. The following is an account of the mating behavioral pathway suggested by the connectivity. When a male touches a hermaphrodite with its tail, a subset of ray neurons stimulates persistent backward locomotion (*21, 22*). At the same time, inputs from other ray neurons place the tail into a ventral curve, pressing it against the hermaphrodite body, a posture maintained throughout mating (*25*). These two activities together constitute the

Response step of mating (*21*). The sharp ventral bend around the end of the hermaphrodite, which occurs if this is reached before the vulva is located, could be manifestation of a different behavioral state (involving PVX or PVV circuitry?) or a different behavioral output of the Response state and arching posture resulting from a change in opposing forces (*47, 58*). When the vulva is located [location of vulva, or Lov, step (*26*)], a new network module, the *Insemination* module, is activated. It is not clear if the *Response* module is deactivated, since all the same sensory inputs to this module remain unchanged, the vulva only adding new inputs. The male could stop at the vulva because flexure of the tail dorsally by contraction of the oblique/gubernacular muscle group causes continued backwards swimming to drive the male against the vulva instead of causing it to slide along the hermaphrodite body (*24*). Alternatively, activity or output of the *Response* module could be inhibited by interactions between modules. For example, the male-specific PVZ interneuron with input from the cloacal sensory neurons, particularly the hook, and output onto the body wall muscle system could be inhibitory to locomotion.

The interpretation of circuitry in the *Insemination* module—which stimulates spicule prodding, spicule insertion, and ejaculation—is supported by experimental analysis (*23, 24, 59*). Inputs from the post-cloacal sensilla activate the gubernacular/oblique muscle group. This group in turn communicates with the spicule protractors and anal depressor via gap junctions and spicule prodding is triggered. If the spicules protract sufficiently, the SPC neurons, which have proprioceptive attachments to the spicule protractor muscles, stop prodding and maintain contraction of the protractor muscles. The sensory neurons with endings opening at the tips of the spicules, SPD and SPV, likely provide the final signal to trigger ejaculation. They send processes into the ventral cord, incompletely reconstructed, that could provide stimulation of the

overlying seminal vesicle to release sperm (*59*). SPD and SPV, as well as the CP(01-06) interneurons (which also have synapses onto the gonad), have extensive output onto body wall muscle and particularly onto the anterior inner longitudinal muscles. The anterior inner longitudinals are a hub of the gap-junction network connecting all the muscles. These gap-junction connections suggest that a general contraction of muscles in the posterior body region may accompany ejaculation.

Finally, an unknown signal terminates the process when insemination has been accomplished and allows the male to withdraw its spicules and swim away. We suggest that the type Ic interneurons may play the role of terminating mating, or of moving the program from the insemination back to the Response step. Type Ic interneurons have output onto the cloacal sensory neurons, the CP(01-06) type Ia interneurons, and the spicule protractor muscles, elements of the insemination circuits (Fig. S11). They receive input from the rays, which promote the earlier Response step of mating, and the hook. Experimental evidence indicates the hook promotes vulva search behavior (Response step) when vulva contact is lost (*24*). One of the type Ic interneurons is the GABAergic DVB interneuron (neurotransmitters in the other type 1c interneurons are not known). Thus, DVB may be inhibitory on its target, the spicule protractor muscles. At the same time, a second class of type Ic interneurons, the DX(01-03) neurons, communicate to the spicule retractor muscles via gap junctions to the dorsal body wall muscles, which in turn make gap junctions onto the spicule retractors (Fig. S11). This constitutes the only synaptic input to the retractors. [The DX(01-03) neurons are unusual in penetrating the basement membrane to directly contact muscle.] As the spicule retractors attach to the dorsal body wall, tensioning of the dorsal body wall muscles along with the spicule retractors may be important for withdrawing the spicules back into the body.

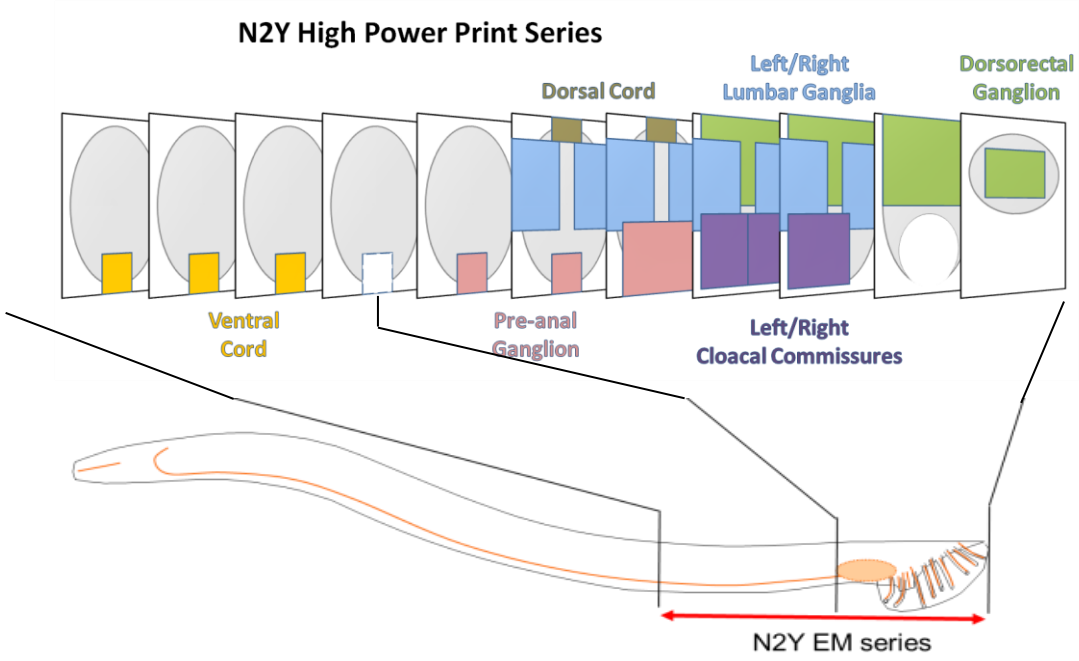

Fig. S1. The N2Y electron micrographs, covering the posterior portion of an adult male. Low power images (grey) cover the entire region every 10-20 sections. High power series taken every 1-3 sections (colors) are used for nervous system reconstruction. The N2Y series is continuous except for a gap of about 30 sections (high power images) between the ventral cord and the pre-anal ganglion (white).

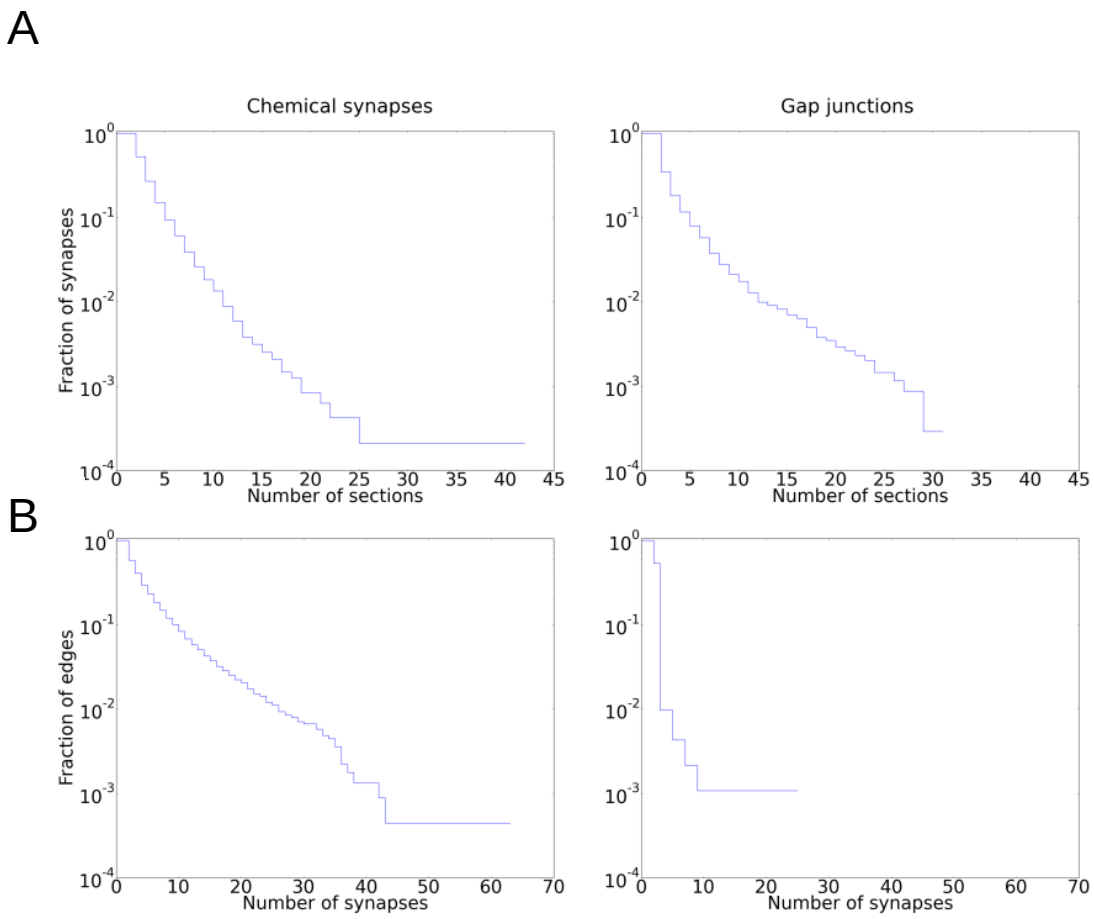

Fig. S2. A. Distributions of sizes of individual presynaptic densities and gap junctions (survival curves). B. Distributions of numbers of chemical and gap junction synapses connecting pairs of cells (number of synapses per edge, survival curves).

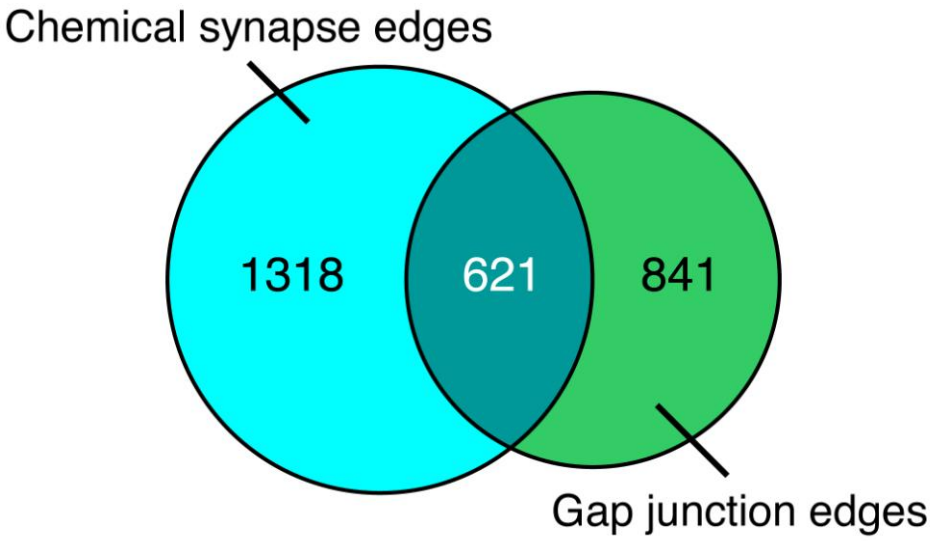

Fig. S3. Relationship of the chemical synapse and gap junction networks for neuron-to-neuron connections. Each gap junction connection is treated as two oppositely directed edges, and autapses are counted. Twenty-two percent of connected neurons are connected by both a chemical and a gap junction edge.

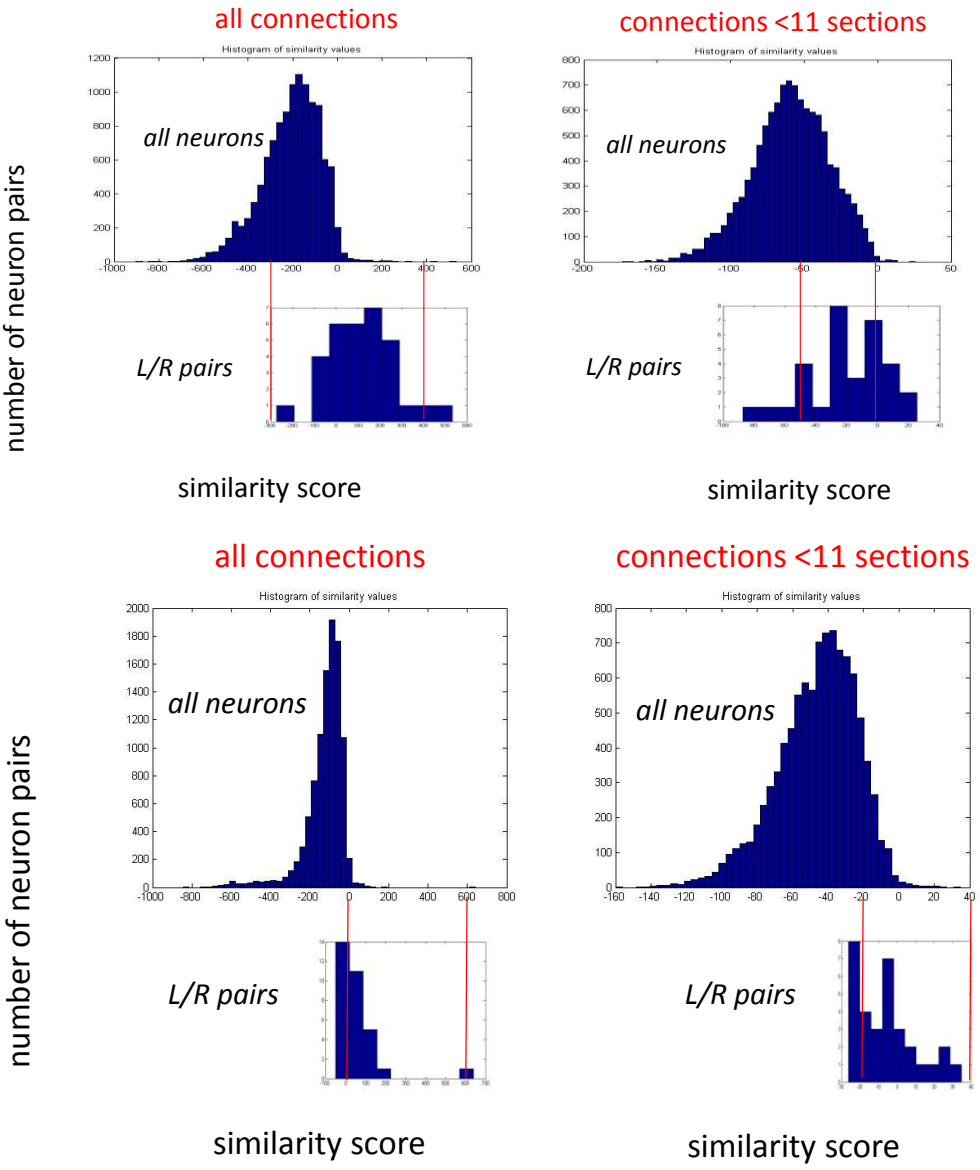

Fig. S4. Distributions of connection similarity scores; *top*: chemical connections, *bottom*: gap junction connections. Even the weaker connections are similar for left/right homologs.

CA(01-06)
CA(07-09)
CP(01-06)
CP(07-09)
DVE, DVF
DX1, DX2, DX3
EF1, EF2, EF3
R1B, R5B, R7B
R2B, R4B, R8B

Fig. S5. Non-left/right pair neurons with high connectivity similarity scores, reciprocal connectivity, often involving gap junctions, and additional reasons for believing they have equivalent function in the network, such as expression of the same neurotransmitter.

Community 1

PCCL, PCCR, SPCL, SPCR, SPDL, SPDR, SPVL, SPVR, CA05, CA06,

Community 2

PHAL, PHAR, PHBL, PHBR, R1BL, R1BR, R3BL, R3BR, R5BR, R6BL, R6BR, R7BL, R7BR, R9BL, R9BR, CA03, CA02,

Community 3

R1AL, R1AR, R2AL, R2AR, R3AL, R3AR, R4AL, R4AR, R5AL, R5AR, R5BL, R6AL, R6AR, R7AL, R7AR, CP07, CP08, CP09, CA04,

Community 4

R2BL, R2BR, R4BL, R4BR, R8AL, R8AR, R8BL, R8BR, R9AL, R9AR, HOA, HOB, PCAL, PCAR, PCBL, PCBR, LUAL, LUAR

Fig. S6. Communities of sensory neurons plus type Ib interneurons, method of Leicht and Newman *(20)*, considering both chemical and gap junction connections. Weights in the gap junction matrix were multiplied by 0.5. Q = 0.469. Average Q for 1000 random graphs = 0.254. std dev = 0.013. $p < 10^{-7}$. Communities 1 and 4 correspond respectively to the Insemination and Response modules. Communities 2 and 3 separate the remaining A and B type ray neurons.

Community 1

R1AL, R1AR, R1BL, R1BR, R2AL, R2AR, R3AL, R3AR, R3BL, R4AL, R4AR, R4BL, R4BR, R5AL, R5AR, R5BL, R5BR, R6AL, R6AR, R6BL, R6BR, R7AL, R7AR, R7BL, R7BR, R8BL, R9BL, R9BR, PVY, AVAL, AVAR, AVBL, AVBR, AVDR, PVCL, PVCR, CP07, CP08, CP09, PDA, PDB, PDC, PVV, CA04, CA07, CA08, CA09, CP04, PGA, AN3a, AN3b, PVNL, PVNR, DA07, DA08, DA09, DB05, DD03, DD06, AS11, VA09, VA10, VA11, VA12, VB06, VB07, VB08, VB09, VB10, VB11, VD09, VD10, VD11, VD12, VD13, PVS, DA04, DA05, DA06, DB04, DB06, DB07, DD04, DD05, AS08, AS09, sph, vBWM, dBWM, dgl, cdl/pol,

Community 2

PHAL, PHAR, PHBL, PHBR, R2BL, R2BR, R3BR, R8AL, R8AR, R8BR, R9AL, R9AR, HOA, HOB, PCAL, PCAR, PCBL, PCBR, PCCL, PCCR, SPCL, SPCR, SPDL, SPDR, SPVL, SPVR, AVG, AVDL, AVL, PVX, LUAL, LUAR, DX1, DX2, DX3, CA02, CA03, CA05, CA06, CP01, CP02, CP03, CP05, CP06, DVB, DVC, DVE, DVF, PVZ, VB05, PVU, PVT, AS10, gonad, grt/gec/aob/pob, vsp/dsp/adp, ail/pil, int,

Fig. S7. Communities generated by the method of simulated annealing *(53)*.

Community 1
vBWM,PVV,VD13,ail/pil,PVZ,dgl,CP04,DD05,CP03,CP02,VA10,VB09,VD11,VB11,
SPDR,VA12,CA05,SPDL,CA04,VA11,VD12,VB10,VB07,CP01,SPVR,VD09,VD10,
CA06,DD04,VB06,DVC,VB08,PVU,SPVL,DB05,CA08,int,DD03,CA09

Community 2
LUAL,LUAR,AVG,grt/gec/aob/pob,PCAL,HOA,PCAR,PVNL,PCBR,R8AR,PCBL,R8AL,
R9AL,R3BR,R2BR,DX3,R8BL,R9AR,R2BL,R4BR,R8BR,PHBR,DX1,R4BL,CA07,
PHBL,PHAL,sph

Community 3
AVAL,PVX,PVY,AVAR,DB07,DB06,VA09,DB04,PVCL,AVBR,DA06,PVCR,DA07,
AVBL,AS09,AS10,DA05,AVDR,AS08,AVDL,DA04,VB05

Community 4
dBWM,DD06,AS11,PDC,PDA,DA09,DA08

Community 5
gonad,adp/dsp/dsr/vsp,AVL,HOB,CP06,DVF,CP05,SPCR,SPCL,DVE,PCCR,PCCL,
DVB,CA03,CA02,PVT

Community 6
PDB,CP07,R6AR,R7AR,CP08,R7AL,R6AL,CP09,PGA,R5BL

Community 7
R9BL,R7BR,R1BR,R7BL,PVNR,R5BR,AN3b,AN3a,R6BR,R9BR,PHAR,PVS

Community 8
R3AL,cdl/pol,R3AR,R1AL

Community 9
R4AL,R4AR,R5AL,R5AR

Community 10
R2AL,R2AR,R1AR

Community 11
R3BL,R6BL,DX2,R1BL

Fig. S8. Communities generated by the random walk method of Rosvall and Bergstrom (*56)*. Neurons and muscle groups are ranked by the fraction of time they are visited by the random walker and are listed in decreasing order.

Ultra-peripheral nodes
PVS DA04 CA02 PVT sph gonad vsp/dsp/adp int DA07 DB05 VA09 VB05 VB07 DA05 DA06 DB04 AS09

Peripheral nodes
R1BL R1BR R3BL R5BL R5BR R6AL R6AR R6BL R6BR R7AL R7AR R7BL R7BR R9BL R9BR CP07 CP08 CP09 PDA PDB PDC PVV PGA AN3a AN3b PVNR VD13 dBWM PHAL PHAR PHBL PHBR R2BL R2BR R3BR R4BL R4BR R8AL R8AR R8BL R8BR R9AL R9AR HOA PCAL PCAR AVG PVY PVX LUAL LUAR DX1 DX3 PVNL HOB PCBL PCBR PCCL PCCR SPCL SPCR CA03 CA06 CP01 CP05 CP06 DVB DVE DVF grt/gec/aob/pob R1AL R1AR R2AL R2AR R3AL R3AR R4AL R4AR R5AL R5AR CA09 cdl/pol SPDL SPDR SPVL SPVR AVAL AVAR AVBL AVDL AVDR PVCR CA08 DVC DA08 DA09 DD03 DD06 VA10 VA11 VA12 VB06 VB08 VB09 VB10 VB11 VD09 VD10 VD11 VD12 DB06 DD04 DD05 AS08 AS10

Non-hub connector nodes
CA04 AS11 AVBR CA07 PVZ AVL DX2 CA05 CP02 CP03 CP04 dgl PVCL PVU DB07 ail/pil

Non-hub kinless nodes, none; Provincial hubs, none; Connector hubs, vBWM; Kinless hubs, none

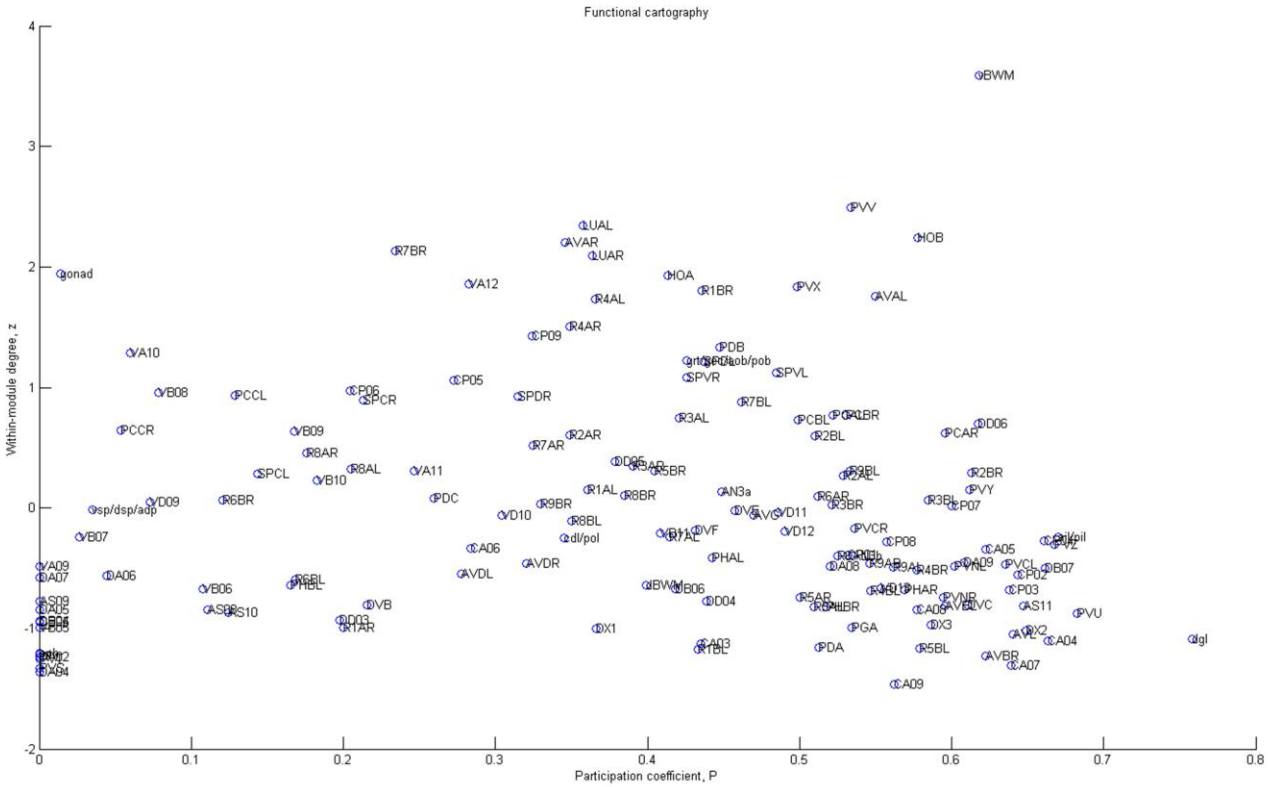

Fig. S9. Partition of the network by the method of functional cartography *(53)*.

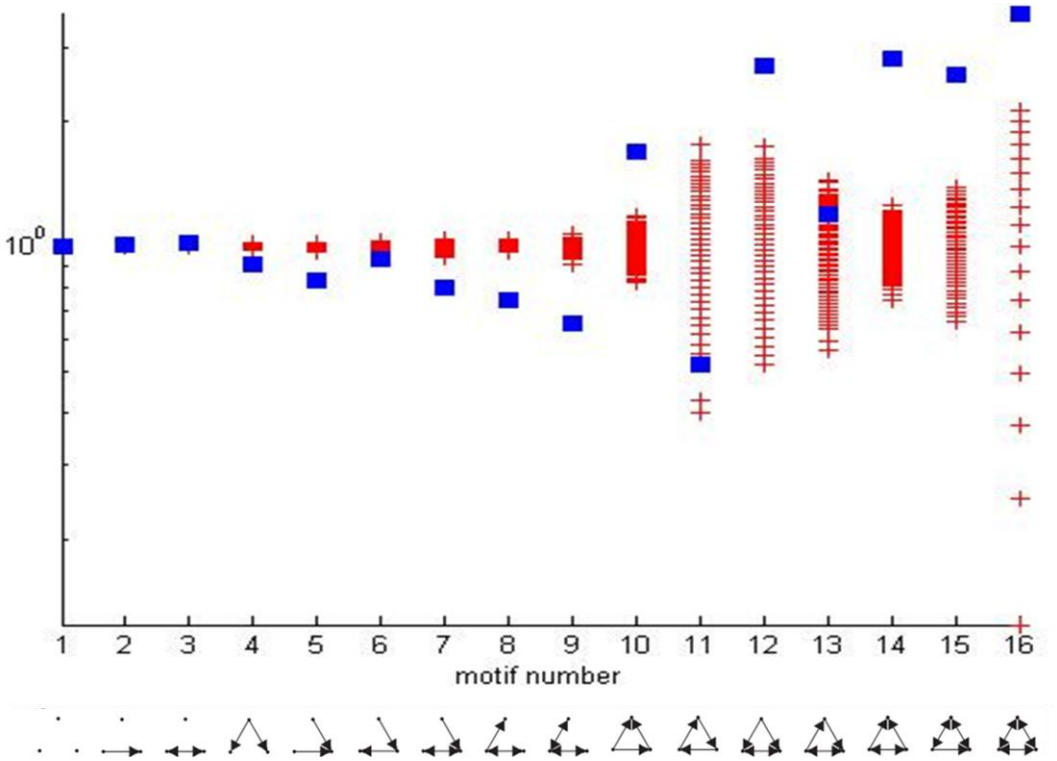

Fig. S10. Triplet motifs. The frequency of triplets in the mating network (blue squares) is compared to the mean obtained from 1000 randomized versions of the network that preserve other network properties (red crosses).

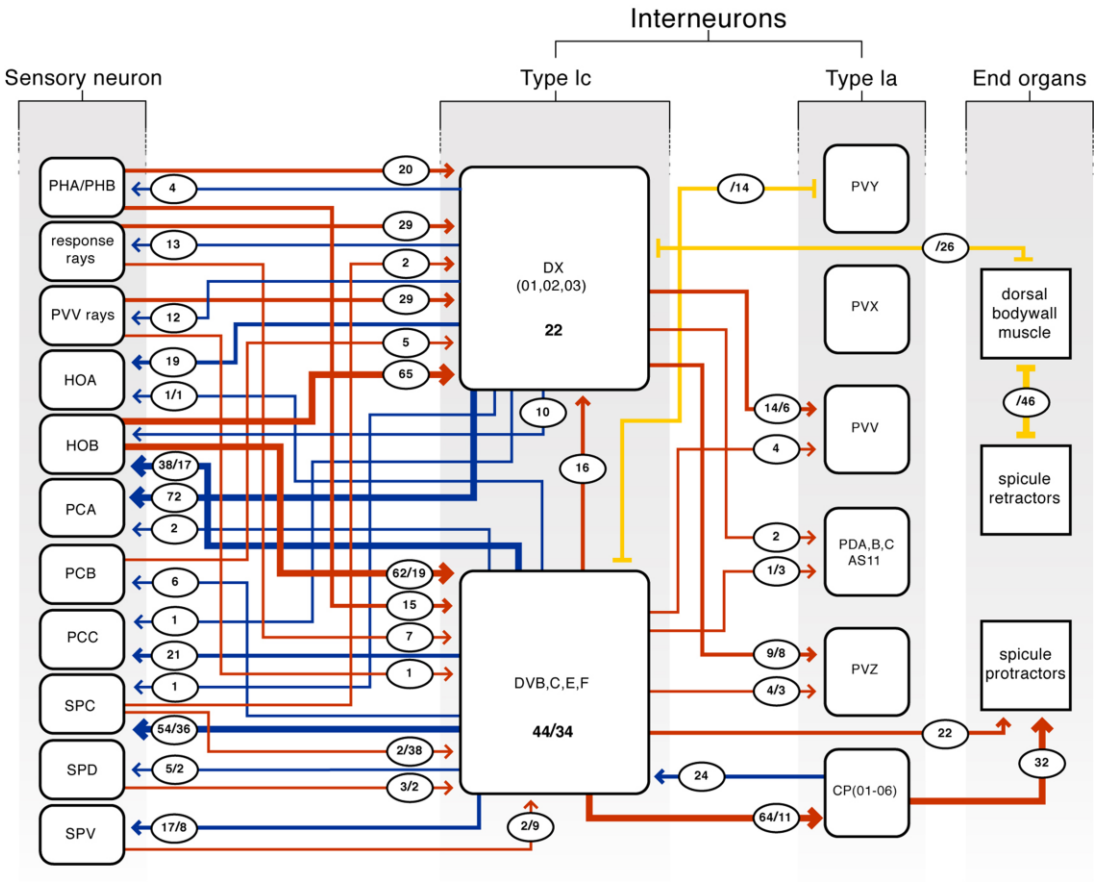

Fig. S11. Detail of circuits involving the Type Ic interneurons.

Table S1 Small world properties of the network sub-graphs. C: clustering coefficient, the average probability that two neurons or muscles that are connected to the same third neuron or muscle are also connected to each other; L: characteristic path length, the average minimum number of steps between pairs of neurons and muscles; C(rand), L(rand): the corresponding values obtained by averaging over a set of appropriately randomized versions of the networks (see methods); S: the ratio of C/C(rand) to L/L(rand). The criterion for "small worldness" is S>1, indicating that the networks have statistically high clustering coefficients when compared to randomized networks while still maintaining short path lengths as found for random networks (59). p values are the probabilities that a randomized network will have a greater clustering coefficient or a longer path length than the actual networks.

sub-graph	C	C(rand)	p	L	L(rand)	p	S
neuron *chemical*	0.336	0.121	0.005	2.46	2.18	$<10^{-7}$	2.46
neuron *gap junction*	0.310	0.094	0.005	2.61	2.41	$<10^{-7}$	3.06
neuron *chem plus gap junction*	0.392	0.148	0.005	2.21	2.05	$<10^{-7}$	2.45
muscle *gap junction*	0.462	0.0376	0.005	3.42	2.57	$<10^{-7}$	9.25

References and Notes

1. J. G. White, E. Southgate, J. N. Thomson, S. Brenner, The structure of the nervous system of the nematode *Caenorhabditis elegans*. *Philos. Trans. R. Soc. Lond. B Biol. Sci.* **314**, 1 (1986).doi:10.1098/rstb.1986.0056 Medline

2. L. R. Varshney, B. L. Chen, E. Paniagua, D. H. Hall, D. B. Chklovskii, Structural properties of the *Caenorhabditis elegans* neuronal network. *PLOS Comput. Biol.* **7**, e1001066 (2011).doi:10.1371/journal.pcbi.1001066 Medline

3. M. de Bono, A. V. Maricq, Neuronal substrates of complex behaviors in *C. elegans*. *Annu. Rev. Neurosci.* **28**, 451 (2005).doi:10.1146/annurev.neuro.27.070203.144259 Medline

4. M. de Bono, M. B. Sokolowski, in *Invertebrate Neurobiology*, G. North, R. J. Greenspan, Eds. (Cold Spring Harbor Laboratory Press, Cold Spring Harbor, NY, 2007).

5. X.-J. Wang, Decision making in recurrent neuronal circuits. *Neuron* **60**, 215 (2008).doi:10.1016/j.neuron.2008.09.034 Medline

6. J. Lipton, G. Kleemann, R. Ghosh, R. Lints, S. W. Emmons, Mate searching in *Caenorhabditis elegans*: A genetic model for sex drive in a simple invertebrate. *J. Neurosci.* **24**, 7427 (2004).doi:10.1523/JNEUROSCI.1746-04.2004 Medline

7. J. M. Simon, P. W. Sternberg, Evidence of a mate-finding cue in the hermaphrodite nematode *Caenorhabditis elegans*. *Proc. Natl. Acad. Sci. U.S.A.* **99**, 1598 (2002).doi:10.1073/pnas.032225799 Medline

8. A. Barrios, S. Nurrish, S. W. Emmons, Sensory regulation of *C. elegans* male mate-searching behavior. *Curr. Biol.* **18**, 1865 (2008).doi:10.1016/j.cub.2008.10.050 Medline

9. J. Q. White *et al*., The sensory circuitry for sexual attraction in *C. elegans* males. *Curr. Biol.* **17**, 1847 (2007).doi:10.1016/j.cub.2007.09.011 Medline

10. J. E. Sulston, D. G. Albertson, J. N. Thomson, The *Caenorhabditis elegans* male: Postembryonic development of nongonadal structures. *Dev. Biol.* **78**, 542 (1980).doi:10.1016/0012-1606(80)90352-8 Medline

11. M. M. Barr, L. R. Garcia, in Neurobiology and behavior section, E. M. Jorgensen and J. M. Kaplan, Eds., *WormBook* (The *C. elegans* Research Community, WormBook 2006); http://www.wormbook.org.

12. L. R. Garcia, B. LeBoeuf, P. Koo, Diversity in mating behavior of hermaphroditic and male-female *Caenorhabditis* nematodes. *Genetics* **175**, 1761 (2007).doi:10.1534/genetics.106.068304 Medline

13. G. A. Kleemann, A. L. Basolo, Facultative decrease in mating resistance in hermaphroditic *Caenorhabditis elegans* with self-sperm depletion. *Anim. Behav.* **74**, 1339 (2007). doi:10.1016/j.anbehav.2007.02.031

14. Neuron maps, synapse lists, and connectivity matrices are available at http://wormwiring.org.

15. S. Brenner, The genetics of *Caenorhabditis elegans*. *Genetics* **77**, 71 (1974). Medline

16. Materials and methods are available as supplementary materials on *Science* Online.

17. D. J. Watts, S. H. Strogatz, Collective dynamics of ‘small-world’ networks. *Nature* **393**, 440 (1998).doi:10.1038/30918 Medline

18. T. Schikorski, C. F. Stevens, Quantitative ultrastructural analysis of hippocampal excitatory synapses. *J. Neurosci.* **17**, 5858 (1997). Medline

19. M. E. J. Newman, Modularity and community structure in networks. *Proc. Natl. Acad. Sci. U.S.A.* **103**, 8577 (2006).doi:10.1073/pnas.0601602103 Medline

20. E. A. Leicht, M. E. J. Newman, Community structure in directed networks. *Phys. Rev. Lett.* **100**, 118703 (2008).doi:10.1103/PhysRevLett.100.118703 Medline

21. K. S. Liu, P. W. Sternberg, Sensory regulation of male mating behavior in *Caenorhabditis elegans*. *Neuron* **14**, 79 (1995).doi:10.1016/0896-6273(95)90242-2 Medline

22. K. Liu, PhD Thesis, California Institute of Technology (1995).

23. L. R. Garcia, P. Mehta, P. W. Sternberg, Regulation of distinct muscle behaviors controls the *C. elegans* male’s copulatory spicules during mating. *Cell* **107**, 777 (2001).doi:10.1016/S0092-8674(01)00600-6 Medline

24. Y. Liu *et al*., A cholinergic-regulated circuit coordinates the maintenance and bi-stable states of a sensory-motor behavior during *Caenorhabditis elegans* male copulation. *PLoS Genet.* **7**, e1001326 (2011).doi:10.1371/journal.pgen.1001326 Medline

25. P. K. Koo, X. Bian, A. L. Sherlekar, M. R. Bunkers, R. Lints, The robustness of *Caenorhabditis elegans* male mating behavior depends on the distributed properties of ray sensory neurons and their output through core and male-specific targets. *J. Neurosci.* **31**, 7497 (2011).doi:10.1523/JNEUROSCI.6153-10.2011 Medline

26. M. M. Barr, P. W. Sternberg, A polycystic kidney-disease gene homologue required for male mating behaviour in *C. elegans*. *Nature* **401**, 386 (1999).doi:10.1038/43913 Medline

27. J. Hertz, A. Krogh, R. G. Palmer, *Introduction to the Theory of Neural Computation, Santa Fe Institute Studies in the Sciences of Complexity* (Westview Press, Boulder, CO,1991).

28. J. J. Hopfield, Neural networks and physical systems with emergent collective computational abilities. *Proc. Natl. Acad. Sci. U.S.A.* **79**, 2554 (1982).doi:10.1073/pnas.79.8.2554 Medline

29. D. Kleinfeld, Sequential state generation by model neural networks. *Proc. Natl. Acad. Sci. U.S.A.* **83**, 9469 (1986).doi:10.1073/pnas.83.24.9469 Medline

30. D. Kleinfeld, H. Sompolinsky, Associative neural network model for the generation of temporal patterns. Theory and application to central pattern generators. *Biophys. J.* **54**, 1039 (1988).doi:10.1016/S0006-3495(88)83041-8 Medline

31. S. Mangan, U. Alon, Structure and function of the feed-forward loop network motif. *Proc. Natl. Acad. Sci. U.S.A.* **100**, 11980 (2003).doi:10.1073/pnas.2133841100 Medline

32. U. Alon, Network motifs: Theory and experimental approaches. *Nat. Rev. Genet.* **8**, 450 (2007).doi:10.1038/nrg2102 Medline

33. H. S. Seung, Reading the book of memory: Sparse sampling versus dense mapping of connectomes. *Neuron* **62**, 17 (2009).doi:10.1016/j.neuron.2009.03.020 Medline

34. O. Sporns, G. Tononi, R. Kötter, The human connectome: A structural description of the human brain. *PLOS Comput. Biol.* **1**, e42 (2005).doi:10.1371/journal.pcbi.0010042 Medline

35. J. W. Lichtman, J. R. Sanes, Ome sweet ome: What can the genome tell us about the connectome? *Curr. Opin. Neurobiol.* **18**, 346 (2008).doi:10.1016/j.conb.2008.08.010 Medline

36. Y. Mishchenko *et al*., Ultrastructural analysis of hippocampal neuropil from the connectomics perspective. *Neuron* **67**, 1009 (2010).doi:10.1016/j.neuron.2010.08.014 Medline

37. D. D. Bock *et al*., Network anatomy and in vivo physiology of visual cortical neurons. *Nature* **471**, 177 (2011).doi:10.1038/nature09802 Medline

38. K. L. Briggman, M. Helmstaedter, W. Denk, Wiring specificity in the direction-selectivity circuit of the retina. *Nature* **471**, 183 (2011).doi:10.1038/nature09818 Medline

39. S. Seung, *Connectome How the Brain's Wiring Makes Us Who We Are*. (Houghton Mifflin Harcourt, Boston, 2012).

40. N. Nagarajan, C. F. Stevens, How does the speed of thought compare for brains and digital computers? *Curr. Biol.* **18**, R756 (2008).doi:10.1016/j.cub.2008.06.043 Medline

41. K. Jezek, E. J. Henriksen, A. Treves, E. I. Moser, M. B. Moser, Theta-paced flickering between place-cell maps in the hippocampus. *Nature* **478**, 246 (2011).doi:10.1038/nature10439 Medline

42. T. J. Wills, C. Lever, F. Cacucci, N. Burgess, J. O'Keefe, Attractor dynamics in the hippocampal representation of the local environment. *Science* **308**, 873 (2005).doi:10.1126/science.1108905 Medline

43. J. Niessing, R. W. Friedrich, Olfactory pattern classification by discrete neuronal network states. *Nature* **465**, 47 (2010).doi:10.1038/nature08961 Medline

44. F. Rosenblatt, The perceptron: A probabilistic model for information storage and organization in the brain. *Psychol. Rev.* **65**, 386 (1958).doi:10.1037/h0042519 Medline

45. S. Haykin, *Neural Networks and Learning Machines* (Pearson Prentice Hall, New York, 2009).

46. M. B. Goodman, D. H. Hall, L. Avery, S. R. Lockery, Active currents regulate sensitivity and dynamic range in *C. elegans* neurons. *Neuron* **20**, 763 (1998).doi:10.1016/S0896-6273(00)81014-4 Medline

47. A. J. Whittaker, P. W. Sternberg, Coordination of opposing sex-specific and core muscle groups regulates male tail posture during *Caenorhabditis elegans* male mating behavior. *BMC Biol.* **7**, 33 (2009).doi:10.1186/1741-7007-7-33 Medline

48. L. D. Peachey, Thin sections. I. A study of section thickness and physical distortion produced during microtomy. *J. Biophys. Biochem. Cytol.* **4**, 233 (1958).doi:10.1083/jcb.4.3.233 Medline

49. V. D. Blondel, A. Gajardo, M. Heymans, P. Senellart, P. Van Dooren, A measure of similarity between graph vertices: Applications to synonym extraction and web searching. *SIAM Rev.* **46**, 647 (2004). doi:10.1137/S0036144502415960

50. M. Reigl, U. Alon, D. B. Chklovskii, Search for computational modules in the *C. elegans* brain. *BMC Biol.* **2**, 25 (2004).doi:10.1186/1741-7007-2-25 Medline

51. L. Jia, S. W. Emmons, Genes that control ray sensory neuron axon development in the *Caenorhabditis elegans* male. *Genetics* **173**, 1241 (2006).doi:10.1534/genetics.106.057000 Medline

52. J. G. White, E. Southgate, J. N. Thomson, S. Brenner, Factors that determine connectivity in the nervous system of *Caenorhabditis elegans*. *Cold Spring Harb. Symp. Quant. Biol.* **48**, 633 (1983).doi:10.1101/SQB.1983.048.01.067 Medline

53. R. Guimerà, L. A. Nunes Amaral, Functional cartography of complex metabolic networks. *Nature* **433**, 895 (2005).doi:10.1038/nature03288 Medline

54. J. Ruan, W. Zhang, Identifying network communities with a high resolution. *Phys. Rev. E Stat. Nonlin. Soft Matter Phys.* **77**, 016104 (2008).doi:10.1103/PhysRevE.77.016104 Medline

55. Y.-Y. Ahn, J. P. Bagrow, S. Lehmann, Link communities reveal multiscale complexity in networks. *Nature* **466**, 761 (2010).doi:10.1038/nature09182 Medline

56. M. Rosvall, C. T. Bergstrom, Maps of random walks on complex networks reveal community structure. *Proc. Natl. Acad. Sci. U.S.A.* **105**, 1118 (2008).doi:10.1073/pnas.0706851105 Medline

57. B. H. Good, Y. A. de Montjoye, A. Clauset, Performance of modularity maximization in practical contexts. *Phys. Rev. E Stat. Nonlin. Soft Matter Phys.* **81**, 046106 (2010).doi:10.1103/PhysRevE.81.046106 Medline

58. C. M. Loer, C. J. Kenyon, Serotonin-deficient mutants and male mating behavior in the nematode *Caenorhabditis elegans*. *J. Neurosci.* **13**, 5407 (1993). Medline

59. G. Schindelman, A. J. Whittaker, J. Y. Thum, S. Gharib, P. W. Sternberg, Initiation of male sperm-transfer behavior in *Caenorhabditis elegans* requires input from the ventral nerve cord. *BMC Biol.* **4**, 26 (2006).doi:10.1186/1741-7007-4-26 Medline

60. M. D. Humphries, K. Gurney, Network 'small-world-ness': A quantitative method for determining canonical network equivalence. *PLoS ONE* **3**, e0002051 (2008).doi:10.1371/journal.pone.0002051 Medline